Nano Research
2024, 17(3): 1281–1287

ISSN 1998-0124 CN 11-5974/O4
https://doi.org/10.1007/s12274-023-6393-4

Research Article

Nanocomposite: Keggin-type Co_4-polyoxometalate@cobalt-porphyrin linked graphdiyne for hydrogen evolution in seawater

Jiejie Ping[1], Danyang He[1], Fei Wang[1], Nan Wang[1], Yi-cheng Fu[3], Zihao Xing[2] (✉), Zhiyu Jia[1] (✉), and Guo-Yu Yang[1] (✉)

[1] *Key Laboratory of Cluster Science, Ministry of Education, School of Chemistry and Chemical Engineering, Beijing Institute of Technology, Beijing 100081, China*
[2] *Key Laboratory of Polyoxometalate and Reticular Material Chemistry of Ministry of Education, Facluty of Chmeistry Northeast Normal University, Changchun 130024, China*
[3] *Peking University Third Hospital, Beijing 100190, China*

Received: 19 October 2023 / **Revised:** 24 November 2023 / **Accepted:** 3 December 2023

ABSTRACT

Polyoxometalate-based nanocomposites with electrocatalytic activity have been applied in hydrogen evolution reactions (HER). Seawater as the main water resource on the earth should be developed as the water electrolysis to prepare high-purity hydrogen. In this paper, we used two synthesis strategies to prepare the nanocomposite Co_4-POM@Co-PGDY (Co_4-POM: the Kegging-type microcrystals of $K_{10}[Co_4(PW_9O_{34})_2]$ and Co-PGDY: cobalt-porphyrin linked graphdiyne) with excellent activity for HER. Co-PGDY as the porous material is applied not only as the protection of microcrystals towards the metal ion in seawater but also as the co-electrocatalyst of Co_4-POM. Co_4-POM@Co-PGDY exhibits excellent HER performance in seawater electrolytes with low overpotential and high stability at high density. Moreover, we have observed a key H_3O^+ intermediate emergence on the surface of nanocomposite during hydrogen evolution process in seawater by Raman synchrotron radiation-based Fourier transform infrared (SR-FTIR). The results in this paper provide an effective strategy for preparing polyoxometalate-based electrocatalysts with high-performance toward hydrogen evolution reaction.

KEYWORDS

polyoxometalate, graphdiyne, seawater, hydrogen evolution reaction

1 Introduction

With the concerns of the global fossil energy crisis, the conflict between economic growth and the environment is becoming more pronounced. It is urgent to explore clean and sustainable energy resources to gradually reduce the use of fossil fuels [1, 2]. High-purity hydrogen (H_2) fuel is an ideal alternative to traditional fossil fuels, with the advantages of high energy density and environmentally friendly [3–5]. In recent years, there has been increasing research on preparation of high-purity hydrogen through electrocatalysis [6–9]. Hydrogen evolution reaction (HER) from water electrolysis, especially from seawater, is one of the most efficient, clean, and sustainable pathways [10–15]. In general, the presence of various dissolved ions and bacteria/microorganisms in seawater could easily poison catalysts, reducing the durability of seawater splitting [16]. It is extremely challenging to develop high-performance HER electrocatalysts that can withstand the effects of low conductivity, high corrosiveness, and physiological saline poisoning. Although platinum-based electrocatalysts have been widely used as high-performance electrocatalysts, their scarcity and poor durability limit their practical application for HER in alkaline electrolytes [17, 18]. Among the various earth-abundant HER catalysts, cobalt-based catalysts have attracted extensive research due to their superior HER performance [19, 20]. Moreover, the Co-based electrocatalysts coated with N-doped carbon or Co, N co-doped carbon have superior HER performance with high stability and high electrical conductivity [21–26]. Polyoxometalates (POMs) as an important area of inorganic chemistry have received too much attention during the past two decades [27]. Due to their all-inorganic nature and various structures, they have a wide range of applications in electrocatalysis and photocatalysis [28–31]. Many POMs-based compounds have been extensively explored for hydrogen evolution reactions [32, 33]. Although the POM-based compounds show outstanding advantages in hydrogen evolution reactions, some issues are still full of challenges. For example, the POM-based electrocatalysts' low stability and catalytic activity hinder their application towards HER in seawater.

Graphdiyne (GDY) as the novel carbon material has a two-dimensional planar and porous structure that is composed of sp^2- and sp-hybridized carbon. The unique structure endows GDY with impressive chemical and physical properties, e.g., highly conjugated system and conductivity, and tunable electronic properties, which lead it to be applied as catalysts [34, 35] and energy conversion [36, 37]. Moreover, The controllable growth of GDY on any substrate provides convenience for its application [38]. Due to the chemical synthesis method of GDY, a series of novel monomers have been used to prepare the derivatives of

Address correspondence to Guo-Yu Yang, ygy@bit.edu.cn; Zhiyu Jia, jzy@bit.edu.cn; Zihao Xing, xingzh612@nenu.edu.cn

GDY, such as Br-GDY and F-GDY. Particularly, nitrogen doping can improve the activity of carbon materials more than other heteroatoms doping. Heteroatom and transition metal doping can significantly improve the electrocatalytic performance of carbon materials [39]. The derivatives of GDY exhibit excellent electrocatalytic activity, which is superior to that of the original GDY [28].

As inspired by the high electrocatalytic activity of Co-added POM and the pioneer study on the derivatives of GDY, a new nanocomposite (Co_4-POM@Co-PGDY) which is composed of the Kegging-type microcrystals of $K_{10}[Co_4(PW_9O_{34})_2]$ (Co_4-POM) and cobalt-porphyrin linked graphdiyne (Co-PGDY) was synthesized on nickel foam (NF). Co-PGDY could benefit from the unique graphdiyne morphology that enhances both corrosion resistance in the electrolyte and intrinsically active CoN_4 sites, which protect the nanocomposite from seawater poisoning for maintaining the electrocatalytic stability [40, 41]. The nanocomposite has superior HER performance with high stability in both 1 M KOH and seawater, which could be attributed to the high electrical conductivity of Co-PGDY with the highly active catalytic site of Co_4-POM. The results provide a way to design the nanocomposite with electrocatalytic activity towards HER in seawater with high stability.

2 Experimental

2.1 Synthesis of Co_4-POM electrode

Co_4-POM was grown on the surface of NF by hydrothermal reaction. First, commercial nickel foam plates (1.5 cm × 1 cm) were washed with acetone, 1 M HCl, ethanol, and deionized water for 5 min, respectively. $Co(NO_3)_2{\cdot}6H_2O$ (0.2 mmol, 0.0582 g), $Na_9[A\text{-}\alpha\text{-}PW_9O_{34}]{\cdot}7H_2O$ (0.1 mmol, 0.2562 g), and KCl (3 mmol, 0.2235 g) were mixed into a 25 mL Teflon autoclave with 10 mL of deionized water. The pH value of the mixed solution was adjusted to 4.5. Second, two pieces of treated nickel foam were put and stirred for 30 min. Furthermore, the Teflon autoclave was heated in the oven at 120 °C for 6 h, then cooled to room temperature and cooled at 4 °C overnight successively. The electrode pieces were washed with deionized water and dried in a vacuum oven at 50 °C. Eventually, the Co_4-POM catalytic material loaded on NF was obtained after drying.

2.2 Synthesis of Co-PGDY electrode

We first synthesized the monomer 5,10,15,20-tetrakis-(4-ethynylphenyl)porphyrin-cobalt (TEPP-Co) (Figs. S1 and S2 in the Electronic Supplementary Material (ESM)). The copper sheet (1 cm × 1 cm) was sonicated with acetone, 1 M HCl, deionized water, and ethanol successively for 5 min. The dried copper sheet and five pieces of nickel foam (1.5 cm × 1 cm) were placed in a 250 mL three-neck flask with 60 mL acetone, 0.6 mL N,N,N',N'-tetramethylethylenediamine (TMEDA) under N_2 atmosphere. Then 25 mg of TEPP-Co was dissolved with 5 mL of pyridine, and the solution was dropped into the three-neck flask. The mixture was refluxed under N_2 atmosphere at 50 °C for one day. After the reaction, the electrode sheet was washed with anhydrous ethanol and dried in a vacuum oven at 50 °C. Then Co-PGDY electrode was obtained after drying.

2.3 Synthesis of Co_4-POM@Co-PGDY electrode

The dried copper sheet and five Co_4-POM electrodes were placed in a 250 mL three-neck flask with 60 mL acetone, 0.6 mL TMEDA under N_2 atmosphere. Furthermore, 25 mg of TEPP-Co was dissolved with 5 mL of pyridine, and the solution was dropped into the three-neck flask. Then the mixture was kept in N_2 atmosphere and refluxed at 50 °C for one day. After the reaction, the electrode pieces were washed with anhydrous ethanol and dried in a vacuum oven at 50 °C. Finally, the Co_4-POM@Co-PGDY electrode was obtained after drying.

3 Results and discussion

As we know, single-atom anchored GDY has exhibited high catalytic activity and stability for hydrogen evolution reactions [42]. Co-PGDY as the effective method to prepare Co-anchored GDY had been applied to use as the electrocatalyst towards oxygen evolution reaction (OER) and oxygen reduction reaction (ORR) [40]. As shown in Fig. 1(a), Co_4-POM@Co-PGDY as the POM-based cluster with Co-anchored PGDY was constructed in two steps. Firstly, the Co_4-POM was synthesized on NF under the hydrothermal method. Secondly, Co-PGDY was synthesized by the polymerization of TEEP-Co under mild chemical conditions. Co-PGDY as the Co atom anchored on PGDY would not only provide another catalytic center for enhancing the catalytic performance of nanocomposite but also have a role of protection for electrode towards the corrosion of electrolyte.

For identifying the structure of the above nanocomposite, a series of characterizations were used to test its physical and chemical properties. The morphological information of Co_4-POM@Co-PGDY was investigated by scanning electron microscopy (SEM). After the hydrothermal reaction, the microcrystal Co_4-POM deposited steadily on the surface of NF (Fig. 1(b)), which provides the prerequisite for optimizing its performance. And then the Co-PGDY growth on the surface of Co_4-POM and NF, which would be used to enhance the conductivity, catalytic activity, and stability of Co_4-POM. Compared with the original Co_4-POM, Co_4-POM@Co-PGDY would have higher catalytic activity towards HER under harsh conditions. Besides the SEM images, transmission electron microscopy (TEM) was further used to investigate the microstructure of Co_4-POM@Co-PGDY. From Fig. 1(d), we observed the microcrystal of Co_4-POM@Co-PGDY, which matches well with the SEM image in Figs. 1(a) and 1(b). As shown in Fig. 1(e), the core–shell structure could be observed clearly in the high-resolution TEM (HRTEM), the thickness of Co-PGDY is close to 10 nm approximately. After a series of attempts, we found that this thickness of Co-PGDY could endow not only better catalytic activity but also more stability. And even more, the lattice fringes of Co_4-POM are exhibited clearly. The lattice spacings of 14.19 and 10.54 nm between two fringes are observed, which should be ascribed to the (200) and (120) planes of the Co_4-POM lattice [43]. For confirming the single Co atom had anchored on Co_4-POM@Co-PGDY, sub-Ångström-resolution, and aberration-corrected scanning TEM (STEM) was used to characterize the morphology of Co-PGDY. Individual heavy atoms can be clearly seen in the atomic resolution high-angle annular dark-field (HAADF) images. Figure 1(f) clearly shows the uniform dispersion of isolated Co atoms (white dots) on the surface of PGDY. Moreover, the scanning TEM and corresponding elemental mapping results (Fig. 1(g)) show the homogeneous distribution of Co, C, N, W, and P over the entire nanosheet.

Except for the morphology information, the chemical composition of Co_4-POM@Co-PGDY had been investigated by powder X-ray diffraction (PXRD) for the bonding environment, crystal structure, and its stability of Co_4-POM during the synthesis of Co-PGDY. To obtain the sample for PXRD, the microcrystal of Co_4-POM@Co-PGDY was removed by ultrasonication in 10 mL ethanol. As shown in Fig. 2(a), the PXRD pattern of the microcrystal matches well with the simulated patterns based on the single crystal data, which means that the Co_4-POM

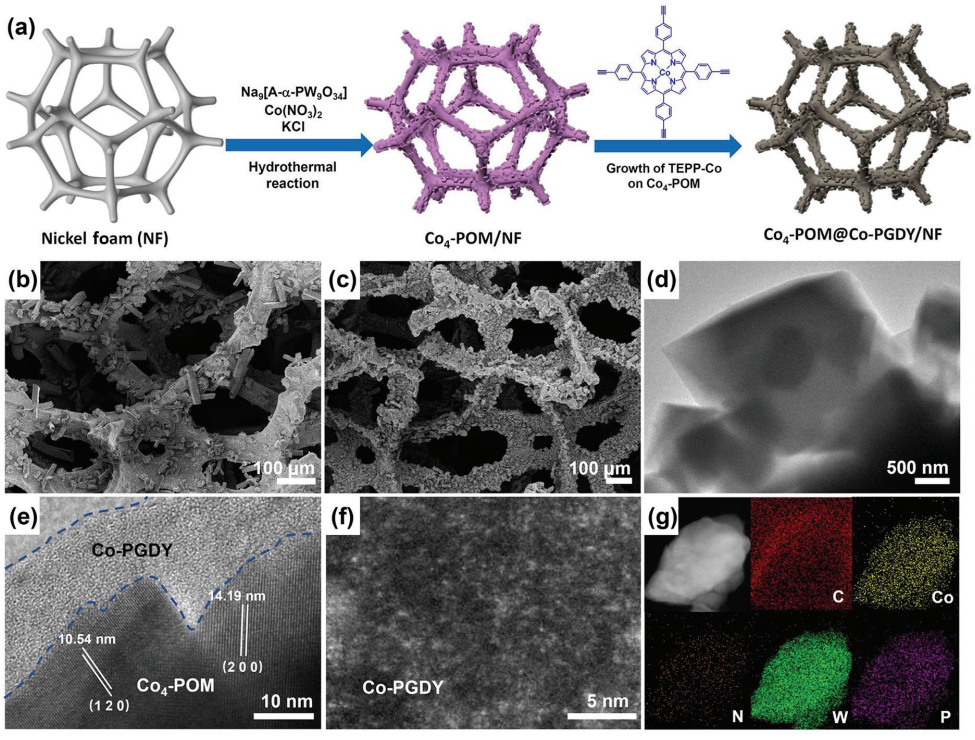

Figure 1 (a) Schematic illustration of preparing Co_4-POM@Co-PGDY electrode. (b) SEM image of Co_4-POM on Ni foam. (c) SEM image of Co_4-POM@Co-PGDY on Ni foam. (d) TEM image of Co_4-POM@Co-PGDY. (e) HRTEM image of Co_4-POM@Co-PGDY, and the corresponding core about Co_4-POM and shell about Co-PGDY. (f) HAADF-STM images of Co-PGDY, reveal that Co atoms are present and uniformly dispersed on PGDY. (g) Scanning TEM image of Co_4-POM@Co-PGDY and corresponding elemental mappings of C, Co, N, W, and P.

microcrystal has a reasonable structure [44]. Moreover, the diffraction spectra of Co_4-POM, Co-PGDY, and Co_4-POM@Co-PGDY further confirm that the microcrystals are stable during the synthesis of Co-PGDY. Furthermore, Raman spectra were used to identify the structure of the Co_4-POM@Co-PGDY. As shown in Fig. 2(b), the peak of Co_4-POM@Co-PGDY at 795.6, 896.4, and 982.6 cm^{-1} is associated with the stretching vibration of the W–O_c–W, W–O_b–W, and W=O_d bond, respectively, which is consistent with that of Co_4-POM; the peak at 1001.1 and 1231.5 cm^{-1} could be attributed to the typical absorption peaks of Co–N and C–N in Co-PGDY. The peaks at 1360.2 and 1545.6 cm^{-1} are contributed by the D band and the G band of the benzene rings in Co-PGDY, respectively. The typical –C≡C– stretching vibration band of 2194.8 cm^{-1} is observed, which is weak because of the molecular perfect symmetry. The peaks at 2357.3 cm^{-1} can be attributed to the vibration of conjugated diyne links (–C≡C–C≡C–) [45]. Therefore, Raman spectrum also indicates the successful preparation of Co_4-POM@Co-PGDY. PXRD patterns and Raman spectrum could be used further to identify that the structure of Co_4-POM is stable during the growth of Co-PGDY.

The valence states of the elements in Co_4-POM@Co-PGDY were determined by X-ray photoelectron spectroscopy (XPS). The XPS spectra of Co_4-POM@Co-PGDY exhibit Co 2p, P 2p, W 4f, O 1s, N 1s, and C 1s compositions in Fig. S3 in the ESM. Four characteristic peaks of Co^{2+} are shown in Fig. 3(a), where the main peak of Co $2p_{3/2}$ is at 781.1 eV and its satellite peak is at 785.5 eV, the main peak of Co $2p_{1/2}$ is at 797.4 eV and its satellite peak is at 803.3 eV. The binding energy of such peaks not only proves the presence of Co^{2+} but also provides evidence to support the formation of CoN_4 [40, 46]. Figure 3(b) exhibits two characteristic peaks of P 2p, whose binding energies are 134.0 eV (P–C) and 134.7 eV (P–O) respectively [47]. Two peaks at 35.8 and 38.0 eV (Fig. 3(c)) can be ascribed to W^{6+} [48]. The O 1s spectrum in Fig. 3(d) is deconvoluted into two peaks; the peak at the binding energy of 530.6 eV belongs to the O=C/O-W bond in POMs; the binding energy of C–O bond is 532.0 eV, which can be attributed to the oxidation of Co-PGDY. Figure 3(e) shows the high-resolution spectra of N 1s. The binding energies of pyridine nitrogen, metal coordination nitrogen, and graphite nitrogen are 398.5, 400.0, and 402.1 eV, respectively [49, 50]. Figure 3(f) shows that the C 1s peaks of Co_4-POM@Co-PGDY can be deconvoluted into three peaks at 284.8, 285.9, and 293.2 eV, centered on graphitic carbon and slightly asymmetric, which is a common feature of N-doped carbon materials [40, 51].

To evaluate the electrocatalytic activity of Co_4-POM@Co-PGDY towards hydrogen evolution reaction in seawater, we first use 1 M KOH as the electrolyte to test its activity. As shown in the Fig. 4(a), Co_4-POM@Co-PGDY as the non-noble metal catalyst exhibits excellent HER performance, the overpotential is smaller (99 mV) than those of Co_4-POM (202 mV), Co-PGDY (121 mV), and NF (219 mV) at the current density of 10 $mA{\cdot}cm^{-2}$, even close to the overpotential of commercial noble metal Pt/C. As shown in Fig. S4 in the ESM, the overpotential of Co_4-POM@Co-PGDY is also only 361 mV at a high current density of 100 $mA{\cdot}cm^{-2}$, which is lower than Co_4-POM (479 mV), Co-PGDY (439 mV), and NF (581 mV). The electrocatalytic activity of Co_4-POM@Co-PGDY could be attributed to the synergistic effect between Co_4-POM and Co-PGDY. As shown in Fig. 4(b), the Tafel slopes of Co_4-POM@Co-PGDY, Co_4-POM, Co-PGDY, and NF are 131, 158, 139 and 181 $mV{\cdot}dec^{-1}$, respectively. The lowest Tafel slope of Co_4-POM@Co-PGDY indicates its superior kinetic performance.

The electrochemically active surface area (ECSA) can be evaluated by the electrochemical double-layer capacitances (C_{dl}), the C_{dl} value is proportional to the ECSA of the catalyst [52]. The values of C_{dl} for different catalysts can be seen in the plot of current density against scan rate (Fig. S5 in the ESM). As shown in Fig. 4(c), the C_{dl} values of Co_4-POM@Co-PGDY, Co_4-POM, and Co-PGDY are 4.46, 1.46, and 1.47 $mF{\cdot}cm^{-2}$, respectively, demonstrating that Co-PGDY helps to expose more catalytically active sites of Co_4-POM. Thus, this proves that Co-PGDY grown on the surface of Co_4-POM can effectively increase the active

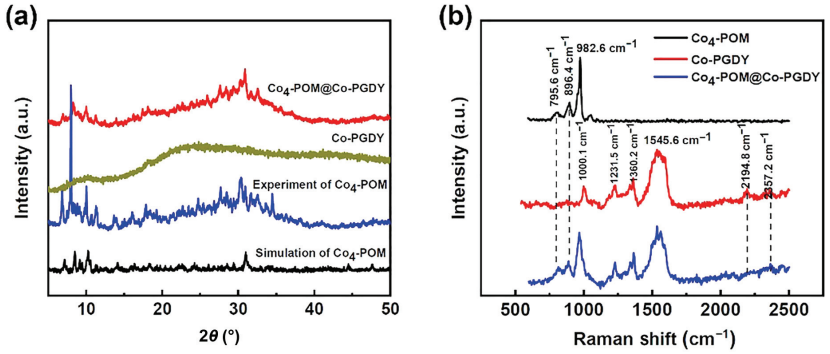

Figure 2 (a) PXRD patterns of Co_4-POM@Co-PGDY, Co-PGDY, and Co_4-POM. (b) Raman spectra of Co_4-POM@Co-PGDY, Co-PGDY, and Co_4-POM.

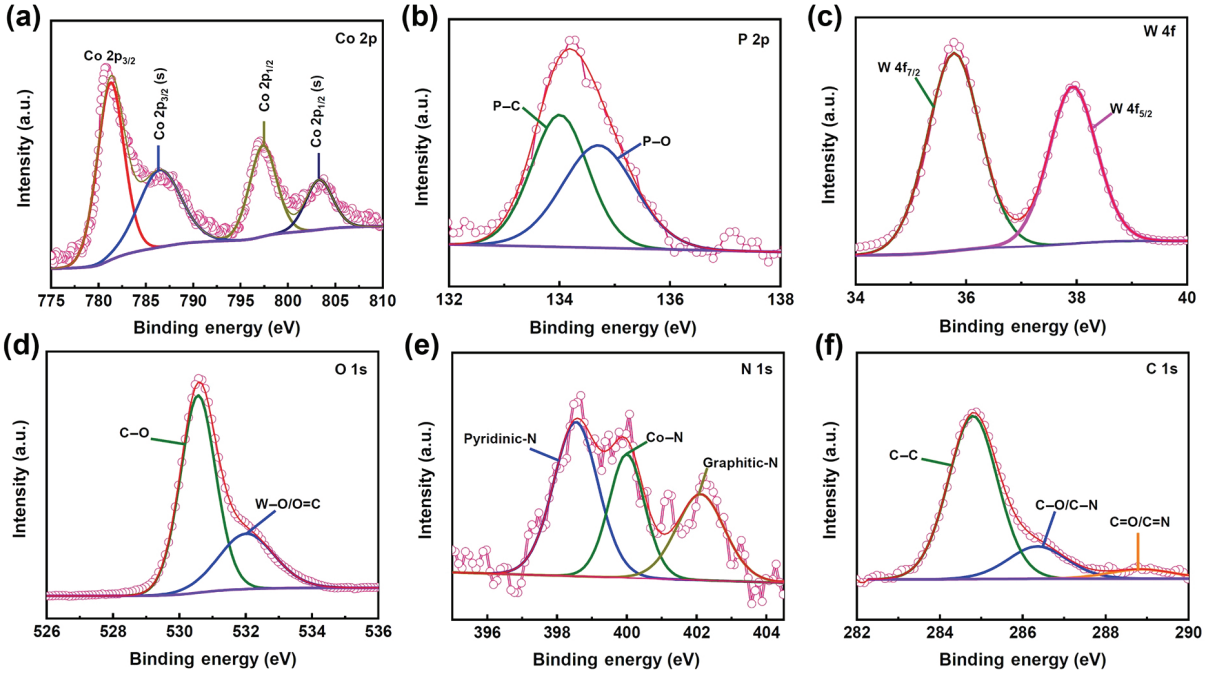

Figure 3 High-resolution XPS spectra of Co_4-POM@Co-PGDY: (a) Co 2p, (b) P 2p, (c) W 4f, (d) O1s, (e) N 1s, and (f) C 1s.

surface area and improve the catalytic activity. Next, we investigated the catalytic kinetics of the reaction at the electrode–electrolyte interface by electrochemical impedance spectroscopy (EIS). The impedance data obtained from the tests were fitted using a circuit model (Fig. S6 in the ESM) to obtain Fig. S7 in the ESM, where the small semicircle in the high frequency range indicates a lower internal resistance and faster charge transfer at the electrode–electrolyte interface [53]. The charge-transfer resistance of Co_4-POM@Co-PGDY is 1.41 Ω, which is smaller than 2.02 Ω for Co_4-POM and 1.71 Ω for Co-PGDY, indicating a faster charge-transfer behavior. This further indicates that the Co_4-POM@Co-PGDY composite has a synergistic effect and the coverage of Co-PGDY enhances the polyacid electrical conductivity, which in turn improves the HER performance and electron transfer rate.

As we know, stability is an important parameter to evaluate the catalytic activity. Figure S8 in the ESM shows the stability of Co_4-POM@Co-PGDY determined by the chrono–current method, with Co_4-POM as the comparison material. After a high current treatment of 100 mA·cm^{-2} for 50 h, the curve of Co_4-POM@Co-PGDY showed a small change, while the current of Co_4-POM without Co-PGDY coverage showed a large change, indicating that the composite cluster has good stability and the coverage of Co-PGDY effectively protects the stability of Co_4-POM. The Co_4-POM@Co-PGDY electrode after HER reaction in 1 M KOH was further investigated by PXRD (Fig. S10(a) in the ESM). The Co_4-POM@Co-PGDY structure remains unchanged before and after HER test, which also indicates its excellent stability in HER cycling.

From the HER performance of Co_4-POM@Co-PGDY in 1 M KOH, we found that Co-PGDY with non-noble metal and porous structure would not only enhance the catalytic activity but also protect the electrocatalyst in harsh conditions. Seawater is the most abundant natural resource on earth and also is a natural multi-component liquid electrolyte. Seawater has a salinity of about 3.5% (35 g·L^{-1}), most of which are Na^+ and Cl^- ions. It has a high ionic conductivity of about 50 mS·cm^{-1} [54]. So we also tested HER performance of the electrocatalysts in seawater (pH = 8.6). As shown in Fig. 4(d), the HER performance of Co_4-POM@Co-PGDY and other contrast electrodes in seawater are the same as that of 1 M KOH, which indicates that the Co_4-POM@Co-PGDY composite cluster has excellent HER catalytic performance in seawater. It is interesting that the overpotential of Co_4-POM@Co-PGDY only requires 301 mV to achieve a current density of 10 mA·cm^{-2}, which is closer to that of Pt/C (279 mV). This is superior to the performance of other catalysts in seawater (Table S1 in the ESM). Moreover, the overpotentials of Co-PGDY and Co_4-POM are 316 and 393 mV, respectively, the above results prove the synergistic electrocatalytic activity between Co_4-POM and Co-PGDY. Figure 4(f) shows that the Tafel slopes of Co_4-POM@Co-PGDY, Co_4-POM, Co-PGDY, and NF are 175, 487, 462, and 609 mV·dec^{-1}, respectively. The lowest Tafel slope indicates the superior kinetic performance of the complex clusters. The superior HER performance in seawater of Co_4-POM@Co-PGDY can be attributed to the enhanced intrinsic activity of the

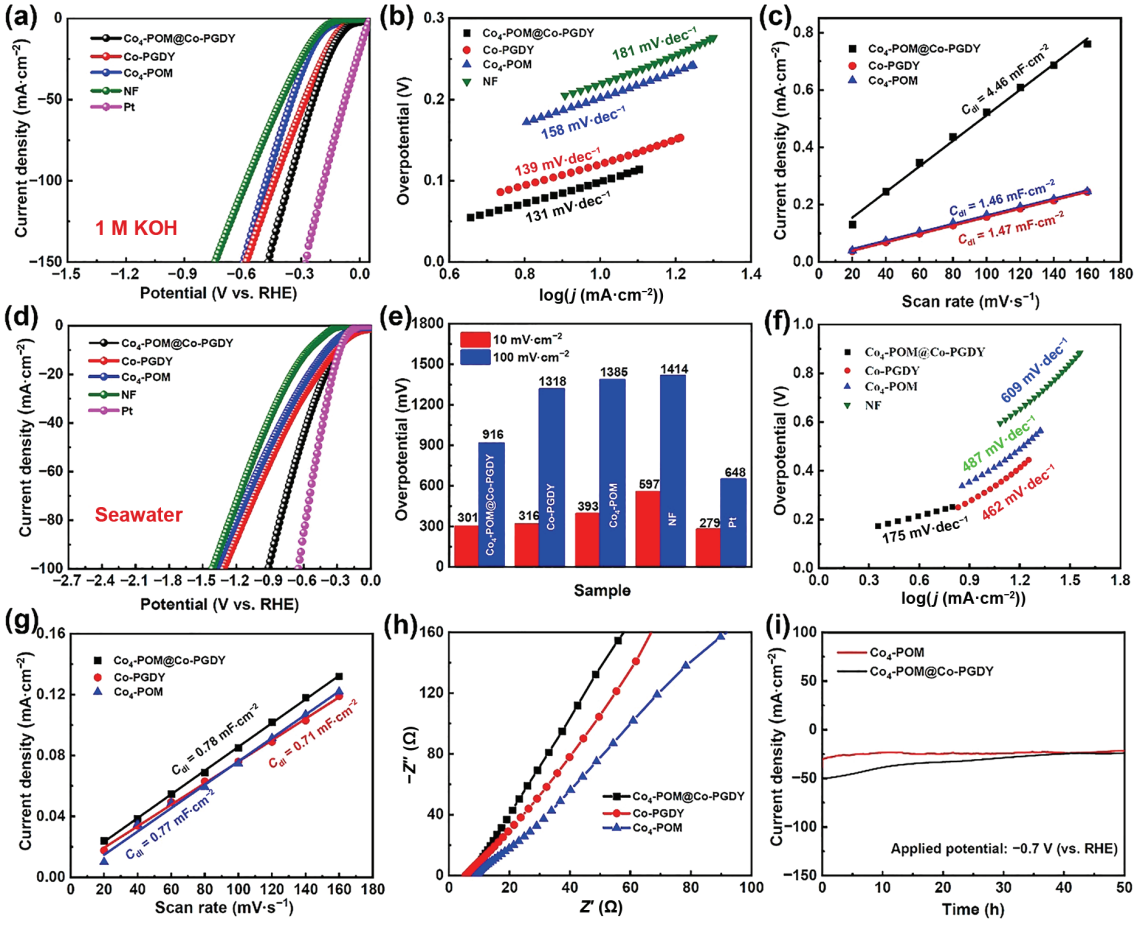

Figure 4 Catalytic performance of Co_4-POM@Co-PGDY in 1 M KOH and seawater: (a) linear sweep voltammetry (LSV) polarization curves of Co_4-POM@Co-PGDY, Co_4-POM, Co-PGDY and NF and (b) the corresponding Tafel slopes. (c) C_{dl} plot of Co_4-POM@Co-PGDY, Co_4-POM, and Co-PGDY; catalytic performance of Co_4-POM@Co-PGDY in seawater: (d) LSV polarization curves of Co_4-POM@Co-PGDY, Co_4-POM, Co-PGDY and NF; (e) table for overpotential at 10 and 100 mA·cm^{-2}; (f) Tafel slopes of Co_4-POM@Co-PGDY, Co_4-POM, Co-PGDY, and NF; (g) C_{dl} plot of Co_4-POM@Co-PGDY, Co_4-POM, and Co-PGDY; (h) EIS Nyquist of Co_4-POM@Co-PGDY, Co_4-POM, and Co-PGDY; (i) time-dependent current density curve of Co_4-POM@Co-PGDY and Co_4-POM.

complex clusters with lower overpotential, more catalytic active sites, and faster HER kinetics.

We get Fig. 4(g) from Fig. S9 in the ESM, which shows the C_{dl} values of Co_4-POM@Co-PGDY, Co_4-POM, and Co-PGDY are 0.78, 0.77, and 0.71 mF·cm^{-2}, respectively. It also implies that Co-PGDY helps to expose more catalytically active sites of Co_4-POM. This also proves that Co-PGDY grown on surface of Co_4-POM can effectively increase the active surface area and improve the catalytic activity. Additionally, the impedance data obtained from the tests were fitted using the same circuit model to obtain Fig. 4(h). The EIS plot shows the charge-transfer resistance of Co_4-POM@Co-PGDY is 1.23 Ω, which is smaller than 5.44 Ω for Co_4-POM and 22.43 Ω for Co-PGDY, indicating a faster charge transfer behavior of their composite clusters, which further indicates the synergistic effect of Co_4-POM@Co-PGDY composites. Figure 4(i) shows the stability of Co_4-POM@Co-PGDY and Co_4-POM measured by the chrono–current method. The current density of Co_4-POM@Co-PGDY catalyst was always greater than that of Co_4-POM after 50 h of treatment at the same voltage, indicating that the composite clusters have better HER stability in seawater. The PXRD pattern (Fig. S10(b) in the ESM) shows the structure of Co_4-POM@Co-PGDY has nearly no change before and after HER testing. The SEM images (Fig. S11 in the ESM) after testing in seawater clearly show that the morphology of Co_4-POM@Co-PGDY is basically unchanged, indicating excellent stability of the composite cluster in seawater. Compared with single component, Co_4-POM@Co-PGDY electrode has a lower overpotential, more accessible active sites, and faster HER kinetics and stability. We further explored the role of Co_4-POM and Co-PGDY. Interestingly, Co-PGDY changed the surface wettability of the electrode. Figure S12 in the ESM shows that Co_4-POM exhibits a super hydrophilicity with a water contact angle nearly 0°, while a decreased hydrophilicity of Co_4-POM@Co-PGDY with a contact angle of 55.2°. This indicates that the coverage of Co-PGDY prevents corrosion of the catalyst by chemical and biological impurities in seawater. Thus the great HER performance of Co_4-POM@Co-PGDY in seawater is promising.

In situ Raman characterization enables us to identify the key acidic intermediates of H_3O^+ of Pt/Co_4-POM@Co-PGDY during the HER process and to monitor their dynamic evolution. The *operando* measurements were conducted under two different conditions: open-circuit (immersed in seawater electrolyte) and the overpotential at 40 mA·cm^{-2} (−0.578 V). Figure 5 shows the Raman spectra of Pt/Co_4-POM@Co-PGDY against the applied potential. From the Raman spectra, we found that the nanocomposite is stable enough. Interestingly, when the applied potential is reduced to 1.327 V vs. RHE, a new peak at ~ 1795 cm^{-1}, which is assigned to H_3O^+ intermediate species, is observed [55], whereas the peak of H_2O (1610 cm^{-1}) becomes weaker and the G-band of graphite (1580 cm^{-1}) remains unchanged, indicating the facilitated water dissociation on the surface of Co_4-POM@Co-PGDY and thereby the generation of abundant H_3O^+ intermediates. The Co_4-POM@Co-PGDY catalyst strongly promotes the water dissociation process and generates a large amount of free H_3O^+ ions under seawater conditions (low [OH^-]).

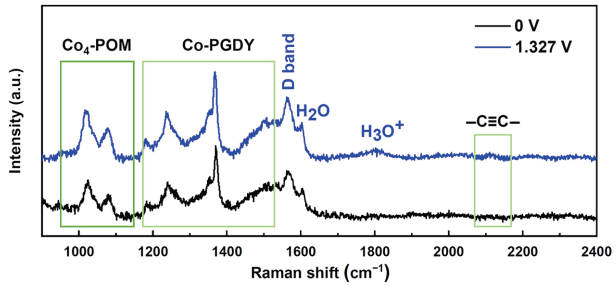

Figure 5 The *operando* Raman SR-FTIR spectra of Pt/Co_4-POM@Co-PGDY at different applied potentials in seawater.

The H_3O^+ intermediates are likely to significantly optimize the proton reduction process by providing an acid-like environment lowering the energy barrier of the overall reaction, thus improving the HER performance.

4 Conclusions

Based on the research of polyoxometalate as the electrocatalyst towards hydrogen evolution reaction, we have concentrated on enhancing its catalytic activity in harsh conditions. We have used two synthesis strategies to prepare the nanocomposite with excellent activity for HER: (i) The transition metal added-POM (Co_4-POM) with the microcrystal structure has electrocatalytic activity superior to that of the original POM; (ii) Co-PGDY as the porous material is applied not only as the protection of microcrystal towards the metal ion in seawater but also as the co-electrocatalyst of Co_4-POM. By testing the HER performance of Co_4-POM@Co-PGDY, we found that the Co_4-POM@Co-PGDY catalysts exhibited low overpotentials of 99 and 301 mV at 10 mA·cm^{-2} in 1 M KOH and seawater, respectively. It also has excellent HER performance at high current densities with great stability. Further, we have identified the key acidic intermediates during the HER process in seawater. Our results provide new insights for the development of low-cost and highly efficient catalysts for seawater splitting.

Acknowledgements

This work was supported by the National Natural Science Foundation of China (Nos. 21831001, 21801014, 22171024, and 22202037) and the Fundamental Research Funds for the Central Universities (No. 2412023QD019). Tests were supported by the Analysis & Testing Center of Beijing Institute of Technology.

Electronic Supplementary Material: Supplementary material (synthesis section, UV–vis spectra, XPS spectra, overpotential table, EIS Nyquist, CV curves, the circuit equivalent model, time-dependent current density curve, PXRD spectra, SEM images, water contact angles, and literature survey table) is available in the online version of this article at https://doi.org/10.1007/s12274-023-6393-4.

References

[1] Turner, J. A. Sustainable hydrogen production. *Science* **2004**, *305*, 972–974.

[2] Chu, S.; Majumdar, A. Opportunities and challenges for a sustainable energy future. *Nature* **2012**, *488*, 294–303.

[3] Song, H. J.; Yoon, H.; Ju, B.; Lee, D. Y.; Kim, D. W. Electrocatalytic selective oxygen evolution of carbon-coated $Na_2Co_{1-x}Fe_xP_2O_7$ nanoparticles for alkaline seawater electrolysis. *ACS Catal.* **2020**, *10*, 702–709.

[4] Chen, W. X.; Pei, J. J.; He, C. T.; Wan, J. W.; Ren, H. L.; Wang, Y.; Dong, J. C.; Wu, K. L.; Cheong, W. C.; Mao, J. J. et al. Single tungsten atoms supported on MOF-derived N-doped carbon for robust electrochemical hydrogen evolution. *Adv. Mater.* **2018**, *30*, 1800396.

[5] Møller, K. T.; Jensen, T. R.; Akiba, E.; Li, H. W. Hydrogen-A sustainable energy carrier. *Prog. Nat. Sci.: Mater. Int.* **2017**, *27*, 34–40.

[6] Wu, J. D.; Wang, D. P.; Wan, S. A.; Liu, H. L.; Wang, C.; Wang, X. An efficient cobalt phosphide electrocatalyst derived from cobalt phosphonate complex for all-pH hydrogen evolution reaction and overall water splitting in alkaline solution. *Small,* **2020**, *16*, 1900550.

[7] Wang, H. Q.; Xu, J. H.; Zhang, Q. B.; Hu, S. X.; Zhou, W. J.; Liu, H.; Wang, X. Super-hybrid transition metal sulfide nanoarrays of Co_3S_4 nanosheet/P-doped WS_2 nanosheet/Co_9S_8 nanoparticle with Pt-like activities for robust all-pH hydrogen evolution. *Adv. Funct. Mater.* **2022**, *32*, 2112362.

[8] Zhang, L. L.; Shi, X. X.; Xu, A. J.; Zhong, W. W.; Zhang, J. T.; Shen, S. J. Novel CoP/$CoMoP_2$ heterojunction with nanoporous structure as an efficient electrocatalyst for hydrogen evolution. *Nano Res.*, in press, https://doi.org/10.1007/s12274-023-6270-1.

[9] Poudel, M. B.; Logeshwaran, N.; Kim, A. R.; Karthikeyan, S. C.; Vijayapradeep, S.; Yoo, D. J. Integrated core–shell assembly of Ni_3S_2 nanowires and CoMoP nanosheets as highly efficient bifunctional electrocatalysts for overall water splitting. *J. Alloys Compd.* **2023**, *960*, 170678.

[10] Wang, Y. D.; Wu, W.; Chen, R. Z.; Lin, C. X.; Mu, S. C.; Cheng, N. C. Reduced water dissociation barrier on constructing Pt-Co/CoO_x interface for alkaline hydrogen evolution. *Nano Res.* **2022**, *15*, 4958–4964.

[11] Jiang, S. H.; Zhang, R. Y.; Liu, H. X.; Rao, Y.; Yu, Y. N.; Chen, S.; Yue, Q.; Zhang, Y. N.; Kang, Y. J. Promoting formation of oxygen vacancies in two-dimensional cobalt-doped ceria nanosheets for efficient hydrogen evolution. *J. Am. Chem. Soc.* **2020**, *142*, 6461–6466.

[12] Wang, S. H.; Wang, L. L.; Xie, L. B.; Zhao, W. W.; Liu, X.; Zhuang, Z. C.; Zhuang, Y. L.; Chen, J.; Liu, S. J.; Zhao, Q. Dislocation-strained MoS_2 nanosheets for high-efficiency hydrogen evolution reaction. *Nano Res.* **2022**, *15*, 4996–5003.

[13] Yu, W. L.; Liu, H. R.; Zhao, Y.; Fu, Y. L.; Xiao, W. P.; Dong, B.; Wu, Z. X.; Chai, Y. M.; Wang, L. Amorphous NiO_n coupled with trace PtO_x toward superior electrocatalytic overall water splitting in alkaline seawater media. *Nano Res.* **2023**, *16*, 6517–6530.

[14] Gao, Y.; Xue, Y. R.; Qi, L.; Xing, C. Y.; Zheng, X. C.; He, F.; Li, Y. L. Rhodium nanocrystals on porous graphdiyne for electrocatalytic hydrogen evolution from saline water. *Nat. Commun.* **2022**, *13*, 5227.

[15] Guo, L. L.; Yu, Q. P.; Zhai, X. J.; Chi, J. Q.; Cui, T.; Zhang, Y.; Lai, J. P.; Wang, L. Reduction-induced interface reconstruction to fabricate $MoNi_4$-based hollow nanorods for hydrazine oxidation assisted energy-saving hydrogen production in seawater. *Nano Res.* **2022**, *15*, 8846–8856.

[16] Tong, W. M.; Forster, M.; Dionigi, F.; Dresp, S.; Sadeghi Erami, R.; Strasser, P.; Cowan, A. J.; Farràs, P. Electrolysis of low-grade and saline surface water. *Nat. Energy* **2020**, *5*, 367–377.

[17] Ma, F. X.; Wu, H. B.; Xia, B. Y.; Xu, C. Y.; Lou, X. W. Hierarchical β-Mo_2C nanotubes organized by ultrathin nanosheets as a highly efficient electrocatalyst for hydrogen production. *Angew. Chem., Int. Ed.* **2015**, *54*, 15395–15399.

[18] Wu, H. B.; Xia, B. Y.; Yu, L.; Yu, X. Y.; Lou, X. W. Porous molybdenum carbide nano-octahedrons synthesized via confined carburization in metal-organic frameworks for efficient hydrogen production. *Nat. Commun.* **2015**, *6*, 6512.

[19] Yang, Y.; Yao, H. Q.; Yu, Z. H.; Islam, S. M.; He, H. Y.; Yuan, M. W.; Yue, Y. H.; Xu, K.; Hao, W. C.; Sun, G. B. et al. Hierarchical nanoassembly of $MoS_2/Co_9S_8/Ni_3S_2$/Ni as a highly efficient electrocatalyst for overall water splitting in a wide pH range. *J. Am. Chem. Soc.* **2019**, *141*, 10417–10430.

[20] Mukhopadhyay, S.; Debgupta, J.; Singh, C.; Kar, A.; Das, S. K. A Keggin polyoxometalate shows water oxidation activity at neutral pH: POM@ZIF-8, an efficient and robust electrocatalyst. *Angew. Chem., Int. Ed.* **2018**, *57*, 1918–1923.

[21] Wang, Z. L.; Hao, X. F.; Jiang, Z.; Sun, X. P.; Xu, D.; Wang, J.; Zhong, H. X.; Meng, F. L.; Zhang, X. B. C and N hybrid

coordination derived Co–C–N complex as a highly efficient electrocatalyst for hydrogen evolution reaction. *J. Am. Chem. Soc.* **2015**, *137*, 15070–15073.

[22] Jin, H. Y.; Wang, J.; Su, D. F.; Wei, Z. Z.; Pang, Z. F.; Wang, Y. *In situ* cobalt-cobalt oxide/N-doped carbon hybrids as superior bifunctional electrocatalysts for hydrogen and oxygen evolution. *J. Am. Chem. Soc.* **2015**, *137*, 2688–2694.

[23] Ni, B.; Zhang, Q. H.; Ouyang, C.; Zhang, S. M.; Yu, B.; Zhuang, J.; Gu, L.; Wang, X. The synthesis of sub-nano-thick Pd nanobelt-based materials for enhanced hydrogen evolution reaction activity. *CCS Chem.* **2019**, *2*, 642–654.

[24] Liu, F.; Shi, C. X.; Guo, X. L.; He, Z. X.; Pan, L.; Huang, Z. F.; Zhang, X. W.; Zou, J. J. Rational design of better hydrogen evolution electrocatalysts for water splitting: A review. *Adv. Sci.* **2022**, *9*, 2200307.

[25] Zhou, B. H.; Gao, R. J.; Zou, J. J.; Yang, H. M. Surface design strategy of catalysts for water electrolysis. *Small* **2022**, *18*, 2202336.

[26] Zhu, H.; Sun, S. H.; Hao, J. C.; Zhuang, Z. C.; Zhang, S. G.; Wang, T. D.; Kang, Q.; Lu, S. L.; Wang, X. F.; Lai, F. L. et al. A high-entropy atomic environment converts inactive to active sites for electrocatalysis. *Energy Environ. Sci.* **2023**, *16*, 619–628.

[27] Miras, H. N.; Yan, J.; Long, D. L.; Cronin, L. Engineering polyoxometalates with emergent properties. *Chem. Soc. Rev.* **2012**, *41*, 7403–7430.

[28] Sun, H.; Xu, X. M.; Jing, C. J.; Shang, W. H.; Wang, Y. C.; Zeng, M. L.; Jia, Z. Y. Composite cluster: $Co_{5.7}Ni_{2.3}W_{12}O_{42}(OH)_4$@fluoro-graphdiyne as a stable electrode for sustained electrochemical oxygen evolution under high current conditions. *Mater. Chem. Front.* **2021**, *5*, 7666–7674.

[29] Li, N.; Liu, J.; Dong, B. X.; Lan, Y. Q. Polyoxometalate-based compounds for photo- and electrocatalytic applications. *Angew. Chem., Int. Ed.* **2020**, *59*, 20779–20793.

[30] Miao, J.; Lang, Z. L.; Zhang, X. Y.; Kong, W. G.; Peng, O. W.; Yang, Y.; Wang, S. P.; Cheng, J. J.; He, T. C.; Amini, A. et al. Polyoxometalate-derived hexagonal molybdenum nitrides (MXenes) supported by boron, nitrogen codoped carbon nanotubes for efficient electrochemical hydrogen evolution from seawater. *Adv. Funct. Mater.* **2019**, *29*, 1805893.

[31] Miras, H. N.; Vilà-Nadal, L.; Cronin, L. Polyoxometalate based open-frameworks (POM-OFs). *Chem. Soc. Rev.* **2014**, *43*, 5679–5699.

[32] Qin, J. S.; Du, D. Y.; Guan, W.; Bo, X. J.; Li, Y. F.; Guo, L. P.; Su, Z. M.; Wang, Y. Y.; Lan, Y. Q.; Zhou, H. C. Ultrastable polymolybdate-based metal organic frameworks as highly active electrocatalysts for hydrogen generation from water. *J. Am. Chem. Soc.* **2015**, *137*, 7169–7177.

[33] Freire, C.; Fernandes, D. M.; Nunes, M.; Abdelkader, V. K. POM & MOF-based electrocatalysts for energy-related reactions. *ChemCatChem* **2018**, *10*, 1703–1730.

[34] Xing, C. Y.; Xue, Y. R.; Huang, B. L.; Yu, H. D.; Hui, L.; Fang, Y.; Liu, Y. X.; Zhao, Y. J.; Li, Z. B.; Li, Y. L. Fluorographdiyne: A metal-free catalyst for applications in water reduction and oxidation. *Angew. Chem., Int. Ed.* **2019**, *58*, 13897–13903.

[35] Xu, X. M.; Wang, Y. C.; Shang, W. H.; Wang, F.; Zhang, Q.; Li, K.; Wu, M.; Jia, Z. Y. Cobalt carbonate hydroxides anchored on nanoscale pyrenely-graphdiyne nanowalls toward bifunctional electrocatalysts with high performance and stability for overall water splitting. *New J. Chem.* **2023**, *47*, 11594–11601.

[36] Kim, K.; Kang, T.; Kim, M.; Kim, J. Three-dimensional entangled and twisted structures of nitrogen doped poly-(1,4-diethynylbenzene) chain combined with cobalt single atom as a highly efficient bifunctional electrocatalyst. *Appl. Catal. B: Environ.* **2020**, *275*, 119107.

[37] Lv, Q.; Wang, N.; Si, W. Y.; Hou, Z. F.; Li, X. D.; Wang, X.; Zhao, F. H.; Yang, Z.; Zhang, Y. L.; Huang, C. S. Pyridinic nitrogen exclusively doped carbon materials as efficient oxygen reduction electrocatalysts for Zn-air batteries. *Appl. Catal. B: Environ.* **2020**, *261*, 118234.

[38] Zheng, X. C.; Chen, S. A.; Li, J. Z.; Wu, H.; Zhang, C.; Zhang, D. Y.; Chen, X.; Gao, Y.; He, F.; Hui, L. et al. Two-dimensional carbon graphdiyne: Advances in fundamental and application research. *ACS Nano* **2023**, *17*, 14309–14346.

[39] Wang, J.; Kong, H.; Zhang, J. Y.; Hao, Y.; Shao, Z. P.; Ciucci, F. Carbon-based electrocatalysts for sustainable energy applications. *Prog. Mater. Sci.* **2021**, *116*, 100717.

[40] Lin, Q. P.; Bu, X. H.; Kong, A. G.; Mao, C. Y.; Bu, F.; Feng, P. Y. Heterometal-embedded organic conjugate frameworks from alternating monomeric iron and cobalt metalloporphyrins and their application in design of porous carbon catalysts. *Adv. Mater.* **2015**, *27*, 3431–3436.

[41] Ma, Y. Y.; Wu, C. X.; Feng, X. J.; Tan, H. Q.; Yan, L. K.; Liu, Y.; Kang, Z. H.; Wang, E. B.; Li, Y. G. Highly efficient hydrogen evolution from seawater by a low-cost and stable CoMoP@C electrocatalyst superior to Pt/C. *Energy Environ. Sci.* **2017**, *10*, 788–798.

[42] Xue, Y. R.; Huang, B. L.; Yi, Y. P.; Guo, Y.; Zuo, Z. C.; Li, Y. J.; Jia, Z. Y.; Liu, H. B.; Li, Y. L. Anchoring zero valence single atoms of nickel and iron on graphdiyne for hydrogen evolution. *Nat. Commun.* **2018**, *9*, 1460.

[43] Finke, R. G.; Droege, M. W.; Domaille, P. J. Trivacant heteropolytungstate derivatives. 3.[1] Rational syntheses, characterization, two-dimensional ^{183}W NMR, and properties of $P_2W_{18}M_4(H_2O)_2O_{68}^{10-}$ and $P_4W_{30}M_4(H_2O)_2O_{112}^{16-}$ (M = Co, Cu, Zn). *Inorg. Chem* **1987**, *26*, 3886–3896

[44] Balula, S. S.; Granadeiro, C. M.; Barbosa, A. D. S.; Santos, I. C. M. S.; Cunha-Silva, L. Multifunctional catalyst based on sandwich-type polyoxotungstate and MIL-101 for liquid phase oxidations. *Catal. Today* **2013**, *210*, 142–148.

[45] Haley, M. M. Synthesis and properties of annulenic subunits of graphyne and graphdiyne nanoarchitectures. *Pure Appl. Chem.* **2008**, *80*, 519–532.

[46] Zhao, Y.; Watanabe, K.; Hashimoto, K. Self-supporting oxygen reduction electrocatalysts made from a nitrogen-rich network polymer. *J. Am. Chem. Soc.* **2012**, *134*, 19528–19531.

[47] Wang, J.; Ciucci, F. *In-situ* synthesis of bimetallic phosphide with carbon tubes as an active electrocatalyst for oxygen evolution reaction. *Appl. Catal B: Environ.* **2019**, *254*, 292–299.

[48] Thilagavathi, T.; Venugopal, D.; Thangaraju, D.; Marnadu, R.; Palanivel, B.; Imran, M.; Shkir, M.; Ubaidullah, M.; AlFaify, S. A facile co-precipitation synthesis of novel WO_3/$NiWO_4$ nanocomposite with improved photocatalytic activity. *Mater. Sci. Semicond. Process.* **2021**, *133*, 105970.

[49] Wu, Z. S.; Chen, L.; Liu, J. Z.; Parvez, K.; Liang, H. W.; Shu, J.; Sachdev, H.; Graf, R.; Feng, X. L.; Müllen, K. High-performance electrocatalysts for oxygen reduction derived from cobalt porphyrin-based conjugated mesoporous polymers. *Adv. Mater.* **2014**, *26*, 1450–1455.

[50] Liang, H. W.; Wei, W.; Wu, Z. S.; Feng, X. L.; Müllen, K. Mesoporous metal-nitrogen-doped carbon electrocatalysts for highly efficient oxygen reduction reaction. *J. Am. Chem. Soc.* **2013**, *135*, 16002–16005.

[51] Yuan, S. W.; Shui, J. L.; Grabstanowicz, L.; Chen, C.; Commet, S.; Reprogle, B.; Xu, T.; Yu, L. P.; Liu, D. J. A highly active and support-free oxygen reduction catalyst prepared from ultrahigh-surface-area porous polyporphyrin. *Angew. Chem., Int. Ed.* **2013**, *52*, 8349–8353.

[52] Voiry, D.; Chhowalla, M.; Gogotsi, Y.; Kotov, N. A.; Li, Y.; Penner, R. M.; Schaak, R. E.; Weiss, P. S. Best practices for reporting electrocatalytic performance of nanomaterials. *ACS Nano* **2018**, *12*, 9635–9638.

[53] Ubaidullah, M.; Al-Enizi, A. M.; Ahamad, T.; Shaikh, S. F.; Al-Abdrabalnabi, M. A.; Samdani, M. S.; Kumar, D.; Alam, M. A.; Khan, M. Fabrication of highly porous N-doped mesoporous carbon using waste polyethylene terephthalate bottle-based MOF-5 for high performance supercapacitor. *J. Energy Storage* **2021**, *33*, 102125.

[54] Hwang, S. M.; Park, J. S.; Kim, Y.; Go, W.; Han, J.; Kim, Y.; Kim, Y. Rechargeable seawater batteries-from concept to applications. *Adv. Mater.* **2019**, *31*, 1804936.

[55] Wang, X. S.; Xu, C. C.; Jaroniec, M.; Zheng, Y.; Qiao, S. Z. Anomalous hydrogen evolution behavior in high-pH environment induced by locally generated hydronium ions. *Nat. Commun.* **2019**, *10*, 4876.